[논문] 한국태양에너지학회 논문집
Journal of the Korean Solar Energy Society
Vol. 25, No. 1, 2005

Feasible Approach for Image Reconstruction in Two Phase Flow Problems

Chun, W.-G., Lee, H.-J., Lee, Y.-J., Kim, M.-C.

Research Institute of Advanced Technology College of Engineering, Cheju National University

이상유동에서의 영상복원을 위한 효율적 기법

천원기, 이윤준, 이헌주, 김민찬

제주대학교 공과대학

Abstract

본 논문은 압력차로 인한 유체의 유동장에서 서스펜션의 입자 밀도를 분포 규명하기 위해 적용할 수 있는 Electric Impedance Tomography (EIT)의 새로운 기법에 대한 효율성을 다루고 있다. Regularized Newton-Raphson iterative method를 근간으로 inverse problem의 해를 구하는데, 이는 곧 목적 함수(object function)를 몇 가지의 제한조건(constraints) 하에서 최소화시키는 과정이라 할 수 있다. 한편, 관련 forward problem은 유한요소법(FEM)을 이용하여 해결하며, 기존의 연구와는 달리 선형 형상 함수(linear shape function)를 이용하여 전도도가 연속적인 물성치로 유동장에 분포되어 있는 것으로 가정하였다. 여러 경우의 test run에 대한 결과는 본 논문에서 적용한 방법론의 타당성을 보여 주고 있다. 태양에너지의 추출을 위해 직접촉식 열교환기가 종종 이용되고 있는데, 본 연구는 열교환기 내부의 분산 유체에 대한 해석에 일조를 할 수 있을 것으로 기대된다.

Keywards : Electric Impedance Tomography (EIT), suspension, dispersed phases, conductivity

1. INTRODUCTION

For years, suspension phenomena attracted many scientists and engineers because of its involvement in many real world problems. These are readily found from those simple examples around us such as food or composite materials. It is also often observed in energy transport processes in nature or engineering plants. A suspension of liquid droplets or fine solid particles in a fluid is witnessed in rivers and oceans as particles remain

suspended so long as energy is applied to the system. In a spray column type direct contact heat exchanger (DCHX), small droplets injected through a sparger from the bottom could form a suspension depending on the operating and physical conditions involved. DCHXs are often used in the solar energy exploitation.

Major efforts are directed in developing new methods to resolve the particle-volume fraction distribution in a suspension experimentally and theoretically. Gadala-Maria and Acrivos (1980) observed a decrease in the suspension viscosity in Couette rheometer. Leighton and Acrivos (1987) showed experimentally and theoretically that the particles migrate from the higher shear regions to the lower ones in Couette rheometer and this migration cause a decrease in the apparent viscosity. Using NMR image, Abbotte *et al.* (1991) found that particles migrate away from the inner cylinder and move toward the outer wall under the low shear rate in Couette rheometer. Many other studies on the particle migration under shear have been conducted by using NMR image [Chow *et al.*, 1994; Mondy *et al.*, 1994; Corbett *et al.*, 1995] and laser Dopler velocimetry (LDV) [Koh *et al.*, 1994; Lyon and Leal, 1998]. The first model of the particle migration under shear was proposed by Leighton and Acrivos (1987). By extending their model, Phillips *et al.* (1992) proposed a new constitutive equation which can measure the actual particle concentration profile. This model predicted the experimental results of particle concentration profile under the Couette and Poiseuille flow quite well.

Recently, EIT technique is employed to investigate two-phase flow phenomena [Reinecke *et al.*, 1988; Butler and Bonnecase, 1999], because it is relatively inexpensive and has good time resolution. In the present study, the shear induced particle migration subjected to a pressure driven flow field is visualized by nonintrusive EIT technique. The proposed image reconstruction algorithm has been tested for several artificial particle concentration distributions where the reconstructed images are compared with those generated by the NMR technique in previous studies.

2. THEORETICAL ANALYSIS

The relationship between the dimensionless conductivity σ_d and volume fraction c_v of suspension was given as [Meredith and Tobias, 1961]

$$c_v = \frac{24 - \left(63 + 448\sigma_d + 64\sigma_d^2\right)^{1/2}}{2\left(8 + \sigma_d\right)} \tag{1}$$

where $\sigma_d = \sigma/\sigma_0$ is the ratio of the conductivity of suspension with respect to that of pure liquid. By using the above equation, the conductivities are converted into particle concentrations. In an EIT system, an array of electrodes are attached on the boundary of an object and small alternating currents are injected through these electrodes and the resulting voltages are measured. Based on these measured data

along the boundary, the internal conductivity (or impedance) distribution can be obtained.

Mathematically, the EIT reconstruction problem is a nonlinear ill-posed inverse problem. The numerical algorithm, which determines the internal conductivity distribution based on the above mentioned boundary data, is not a straight forward one. It requires an iterative procedure of solving a forward problem with the newly-computed conductivity distribution from an inverse problem. The forward problem of EIT calculates the boundary voltages by using an assumed conductivity distribution, and the inverse problem reconstruct the conductivity distribution by using boundary voltage measurements. The details of the forward and inverse problems are discussed below.

2.1 Forward Problem

When the conductance distribution $\sigma(x,y)$ and boundary current density I are given, the voltage distribution ϕ within and on the object boundary is governed by the following Laplace equation and the Neumann type boundary conditions:

$$\nabla \cdot \sigma \nabla \phi = 0 \tag{2}$$

$$\sigma \frac{\partial \phi}{\partial n} = I \quad \text{on the electrodes} \tag{3}$$

where n is the outward directed normal vector.

Since the above equation can't be solved analytically for an arbitrary conductivity distribution, the numerical method such as FEM method should be employed to obtain the solutions. In most of EIT problems, the conductivity(or impedance) within the element assumed to be constant, that is the conductivity distribution is considered to be piecewise continuous. This enables the above differential equation to be expressed in the following algebraic equations:

$$[Y]_{N\times N}[\phi]_{N\times 1} = [c]_{N\times 1} \tag{4}$$

where N is the number of nodes. The global stiffness matrix Y is very sparce, which requires a sparce matrix solver. The solver should handle any sparcity in a matrix without undue difficulties. Now, the voltage distribution can be approximated by the solution of the above algebraic equation. The details of matrix Y, and vectors and c are given in Woo (1990).

Butler and Bonnecaze (1999) assumed that the particle concentration within the element be constant and the conductivity values of the elements in any ring be the same. Based on this assumption, they used 4 electrode arrays and reconstructed the particle concentration profile by employing a three-dimensional inverse algorithm using 10 terms of the two-dimensional (2-D) model. The size of stiffness matrix of the 3-D model is much larger than the 2-D model. If 10 terms of the 2-D model are used in the 3-D model, the size of the stiffness matrix of the 3-D model is 10×10 times larger than that of the 2-D model. Therefore, the computational load of the 3-D model is much heavier. In this study, it is assumed that the conductivity be continuous within the entire domain and

varies only with the radial position. The conductivity distribution is approximated as follows:

$$\sigma(x,y)=\sum_{i=1}^{N}\sigma_i\varphi_i(x,y)=\sum_{i=1}^{N}\sigma_i\varphi_i(r) \quad (5)$$

where φ_i is the interpolation function. If the simplest case is chosen which could be characterized by a triangular element, a bilinear shape function for ϕ and a bilinear interpolation function for σ, the discontinuity of conductance distribution is readily resolved. This also results in a slight change in the structure of matrix Y by adopting $\sigma^e=(\sigma_1^e+\sigma_2^e+\sigma_3^e)/3$, where σ^e is the conductivity of e-th element, and σ_i^e is the conductivity of i-th node in e-th element . The proposed continuous conductivity model is more physically realistic than Butler and Bonnecaze's (1999) piecewise continuous model since the conductivity is a continuous function of radial position, especially, in this problem. The conductivity values of nodes in any ring are set to their average value after each iteraton to enforce the radial conductivity profile.

2.2 Inverse Problem

The inverse problem of EIT maps the boundary voltages from real or artificial experiments to conductivity images. The objective function may be chosen to minimize the square error,

$$\Phi(\sigma)=1/2[v(\sigma)-V_0]^T[v(\sigma)-V_0] \quad (6)$$

where V_0 is the vector of measured voltage and $v(\sigma)$ is calculated boundary voltage vector which should be manipulated to match V_0.

To find σ, which minimizes the above object function, its derivative is set to zero:

$$\Phi'(\sigma)=[v'(\sigma)]^T[v(\sigma)-V_0]=0 \quad (7)$$

where $[v']_{ij}=\frac{\partial v_i}{\partial \sigma_j}$ is the Jacobian matrix. For the solution of the above eqn. (7), the Newton-Raphson linearization is brought in for the conductivity vector σ^k as shown in the following:

$$\Phi'(\sigma^{k+1})=\Phi'(\sigma^k)+\Phi''(\sigma^k)(\sigma^{k+1}-\sigma^k)=0$$

The term Φ'' is called the Hessian matrix, which is expressed as

$$\Phi''=[v']^T v'+[v'']^T\{I\otimes[v-V_0]\} \quad (8)$$

where $\otimes$ is the Kronecker matrix product. Since v'' is difficult to calculate and relatively small, the second term in the above equation is usually omitted. Therefore the Hessian matrix is modified as

$$\Phi''=[v']^T v' \quad (9)$$

The Hessian matrix is known to be ill-conditioned, which could interfere with the performance of image reconstruction algorithm. To overcome this problem, the

object function which should be minimized, is regularized as:

$$\Phi(\sigma)=1/2\left\{[v(\sigma)-V_0]^T[v(\sigma)-V_0]+\alpha(L\sigma)^T(L\sigma)\right\} \quad (10)$$

where L is regularization matrix and is a regularization parameter. The most often used regularization matrix is identity matrix [Hua, *et al.*, 1988]. The iterative equation to refresh the conductivity vector based on the above regularized object function is derived as

$$\sigma^{k+1}=\sigma^k+\Delta\sigma^k \quad (11.a)$$

$$\Delta\sigma^k=H^{-1}\left\{J^T(V_0-v(\sigma^k))-\alpha L^TL\sigma^k\right\} \quad (11.b)$$

$$H=J^TJ+\alpha L^TL \quad (11.c)$$

where J and H are the Jacobian and the modified Hessian matrix, respectively.

There are various regularization algorithms (Vauhkonen, 1997). In commonly used algorithm, the increment of conductivity vector is given as

$$\Delta\sigma^k=\left(J^TJ+\alpha L^TL\right)^{-1}\left[J^T(V_0-v(\sigma^k))\right] \quad (12)$$

where $L^TL=\mathrm{diag}(J^TJ)$ in NOSER algorithm [Cheney *et al.*, 1990], $L^TL=I$ (identity) in Levenberg-Marquadt algorithm [Hua *et al.*, 1988] and $L^TL\sigma$ term is enforced to be zero vector. In these cases, the regularization matrix is regarded as to represent an approximation for the second term in Hessian matrix. In these algorithems, the convergence becomes worse if $L^TL\sigma$ terms are considered.

In the subspace regularization method, the regularization matrix L is chosen to be the null space of conductivity vector, $L=\mathrm{null}(\sigma)$. In this choice, $L^TL\sigma$ term naturally becomes zero vector and the increment of conductivity vector is given as in eqn. (12). Vauhkonen et al. (1998) have shown that the subspace regularization yields more realistic reconstruction which could handle measurement errors more efficiently. This approach of the subspace regularization is used in this study. The regularization parameter α is a large positive value which changes accordingly with the iterative solution procedure. If $\alpha=0$, this regularization scheme turns into the Newton-Raphson method.

The following root-mean-squared global error (ε) is defined to check the convergence of the inverse problem:

$$\varepsilon=\sqrt{\frac{(v-V_0)^T(v-V_0)}{V_0^TV_0}} \quad (13)$$

If ε is less than the predetermined small value, convergence is assumed and the reconstruction is terminated. In this study, $\varepsilon=10^{-3}$ is adopted. If ε decreases, the regularization parameter α decreases rapidly, and vice versa.

2.3 Calculation of the Jacobian Matrix.

The iteration procedure of the inverse problem requires the resolution of the forward problem as it is necessary to obtain

the boundary voltagesand the Jacobian matrix. The Jacobian matrix for the k-th current pattern

$$J_k = \left[\frac{\partial v_i^k}{\partial \sigma_j}\right] = T\left[\frac{\partial \phi_i^k}{\partial \sigma_j}\right] \text{ is obtained as}$$

$$\frac{\partial \phi_i^k}{\partial \sigma_j} = \frac{\partial Y}{\partial \sigma_j} c_i^k = -Y^{-1}\frac{\partial Y}{\partial \sigma_j} Y^{-1} c_i^k = -Y^{-1}\frac{\partial Y}{\partial \sigma_j} Y^{-1}\phi_i^k \tag{14}$$

where T is a transformation matrix, which extracts the boundary informations. The matrix and vectors used in the above equation is given in eqn. (4). The full Jacobian matrix is given as

$$J = \left[J_1^T, J_2^T, K, J_{P-1}^T, J_P^T\right]^T \tag{15}$$

where P is the number of injected current patterns. Therefore the size of the Jacobian matrix is $((L-1)\times P)\times N$, where L, P, N indicate the number of electrodes, current patterns, and nodes, respectively. If one of the electrodes is chosen as a reference electrode, there are only (L-1) voltages for each current pattern. In the piecewise continuous model, such as Butler and Bonnecaze's (1999), the size of Jacobian matrix is $((L-1)\times P)\times E$, where E is the number of element and $E > N$. The size of Jacobian matrix of the present continuous model is smaller than that of the Butler and Bonecaze's (1999) piecewise continuous model. This manifests that the present model could become more computationally efficient than the Butler and Bonnecaze's approach.

There are many data collecting methods such as neighboring method, cross method, opposite method, multi-reference method and adaptive method. The characteristics of these methods are summarized in Webster's (1990). Of these, the adaptive method, which yields the desired current distribution simply by simultaneously injecting currents through all the electrodes, is known to be the best method. In this study, we use FEM grid given in Fig. 2 and inject $P = 16$ simple current patterns into L=32 electrodes simultaneously as follows:

$$I_l^k = \begin{cases} \sin(k\zeta_l) \\ \cos(k\zeta_l) \end{cases} \quad l = 1,2,\Lambda\ ,L/2 \text{ and } k = 1,2,\Lambda\ ,P \tag{16}$$

where $\zeta_l = 2\pi l/L$.

Based on the theoretical background, actual experimentations could be made on a DCHX. Fig. 1 gives an example of the measurement section with 32 electrodes.

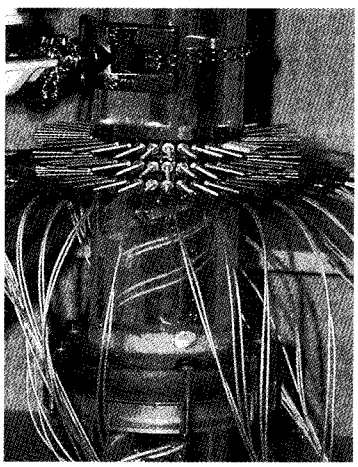

Fig. 1. A measurement section set up in a spray column type direct contact heat exchanger(DCHX)

3. RESULTS AND DISCUSSION (RECONSTRUCTION OF PARTICLE DISTRIBUTION)

The resolution of the EIT system depends on various variables, such as the conductivity contrast and its distribution, injected current patterns, and the errors in voltage measurements. This calls for a verification test to assess the appropriateness of the present EIT technique. A series of simulation has been carried out in this regard.

To investigate the effect of the conductivity distribution on the resolution of reconstructed images, an artificial conductivity distribution is assumed with which the synthetic boundary voltages are obtained by using the forward solver described earlier. In this study, identical values are enforced for the conductivities at the same radial positions and the two-dimensional inverse algorithm described above is adopted. The results of such examples are shown in Figs. 2-5. The conductivity profile in the first example, as shown in Fig. 2, has a step change at $r/R = 0.5$. The reconstructed profile matches the original profile near the wall very well, and accurately predicts its location of a step change. The deviation near the center is an indication that the cause(the change of conductivity vector)-and-effect(the boundary voltages) relation is rather dull in contrast to what's been observed near the wall. Similar behaviors are also observed for the other case as shown in Fig. 3, which includes two large step changes in the original conductivity distribution.

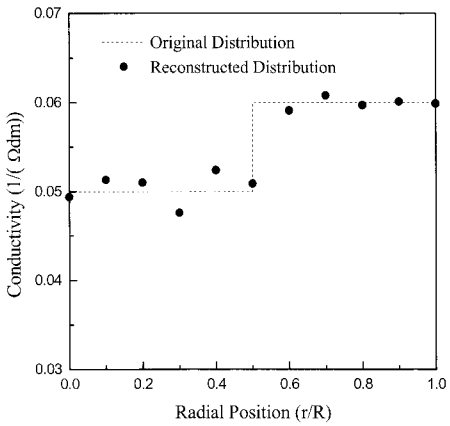

Fig. 2. Computer simulation result of example 1.

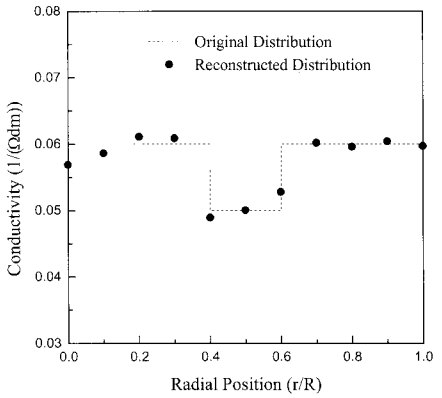

Fig. 3. Computer simulation result of example 2.

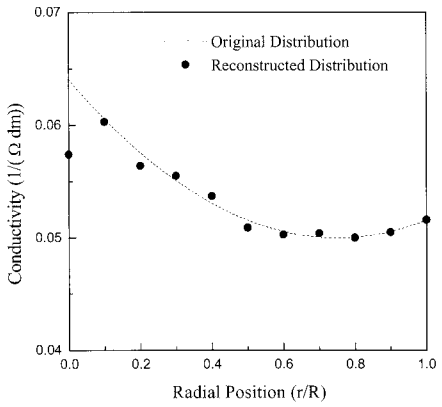

Fig. 4. Computer simulation result of example 3.

For the shear-induced particle migration in a suspension, it deems valid to assume a continuous conductivity distribution. The third example in Fig. 4 shows a shallow dip in its distribution curve with a small difference in its maximum and minimum values. Especially, the reconstructed image tracks the original image fairly well. The last of the simulation examples is given in Fig. 5. where the distribution curve shows a monotonic increase of conductivity as its radial position gets closer to the wall. It also features a relatively large contrast ratio. The conductivity value almost triples as it varies from the center to the wall. The reconstructed image is in a good agreement with the original one except near the center. These results are quite comparable to those produced by Butler and Bonnecaze's (1999) 3-D model and much better than their 2-D results. However, a direct comparison with the Butler and Bonnecaze's model deems impossible as they used a piecewise continuous conductivity model different from the present continuous conductivity model.

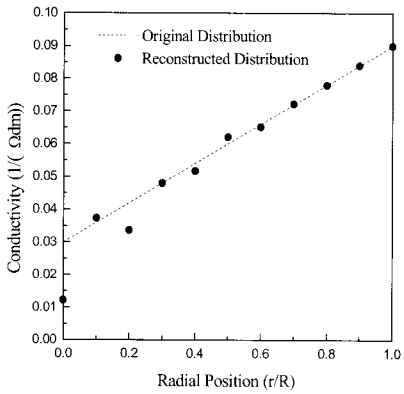

Fig. 5. Computer simulation result of example 4.

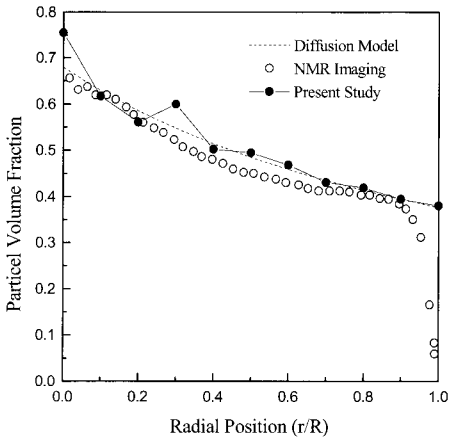

Fig. 6. Comparison between the simulation resultwith theory (Phillips, et al., 1992) and NMR imaging (Hampton, et al., 1997) for the case of average volume fraction $\langle c_v \rangle = 0.45$.

The particle volume-fraction distribution under shearing has been investigated theoretically and experimentally. The particle concentration distributions determined by the diffusion model [Phillips, *et al.*, 1992] and NMR image [Hampton, *et al.*, 1997] are summarized in Fig. 6. Based on the outcome of the diffusion model and eqn. (1), the original conductivity distribution is obtained and the numerical simulation has been carried out to reconstruct the conductivity distribution. Fig. 6. shows a comparison of the simulation results with the NMR images. As shown in this figure, the particle concentration distribution reconstructed by the EIT technique agrees quite well with the other methods except near the inner region.

This discrepancy demonstrates the weakness of the cause-and-effect relationship within the inner region.

4. CONCLUSIONS

A numerical algorithm is proposed to obtain the particle concentration profile in a suspension subjected to a pressure driven flow field by using the EIT technique. On the basis of the geometry, the axially symmetric flow field, and the continuity of the particle concentration distribution, an axially symmetric node-wise reconstruction algorithm has been developed and tested. To establish its reliability, comparisons are made with other methods and the results are analyzed in this regard. It appears that the method could be easily applied to study the dispersed fluid in a direct contact heat exchanger (DCHX) often used for solar energy exploitation.

ACKNOWLEDGEMENTS

This work was supported by the Ministry of Science and Technology (MOST).

REFERENCES

1. Abott, J.R., et al.(1999). "Experimental Oservations of Prticle Mgration in Cncentrated Suspensions: Couette Flow," *J. Rheol.*, 35, 773 .
2. Butler, J.E., et al. (1991). "Imaging of Particle Shear Migration with Electric Impedance Tomography," *Phys. Fluid*, 11, 1982 .
3. Cheney, M. (1990). "NOSER: An Algorithm for Solving the Inverse Conductivity Problem," *Int. J. Imaging Systems and Tehchnology*, 2, 66.
4. Chow, A.W., et al. (1994). "Shear-Induced Migraton in Couette and Parallel-Plate Viscometers: NMR Imaging and Stress Measurements," *Phys. Fluids*, 6, 2561.
5. Corbett, A.M., et al. (1995). "Magnetic Resonance Imaging of Concentration and Velocity Profiles of Pure Fluid and Solid Suspensions in Rotating Geometrues," *J. Rheol.*, 39, 907.
6. Gadala-Maria, F., et al. (1980). "Shear-Induced Structure in a Concentrated Suspension of Solid Sphere," *J. Rheol.*, 24, 799.
7. Hampton, R.E., et al. (1997). "Migration of Particles Undergoing Pressure-Driven Flow in a Circular Conduit," J. Rheol., 41, 621.
8. Hua, P., et al. (1988). "A Regularised Electric Impedance Tomography Reconstruction Algorithm," *Clin. Phys. Physiol. Meas.*, 9 Suppl. A, 137.
10. Koh, C.J, et al. (1994). "An Experimental Investigation of Concentrated Suspension Flows in a Rectangular Channel Flow," *J. Fluid Mech.*, 363, 1.
11. Leighton, D., et al. (1987). " The Shear-Induced Migration of Particles in Concentrated Suspensions," *J. Fluid Mech.*, 181, 415.
12. Meredith, R.E., et al. (1961). "Conductivities in Emulsion," *J. Electrochem. Soc.*, 108, 286.
13. Lyon, M.K., et al. (1998). "An Experimental Study of the Motion of Concentrated Suspensions in Two-Dimensional Channel Flow. Part 1. Mono-Dispersed System," *J. Fluid Mech.*, 363, 25.

14. Mondy, L.A., et al. (1994). "Shear-Induced Particel Migrationin Suspension of Rod," *J. Rheol.*, 38, 444 .
15. Phillips, R.J., et al. (1992). "A Constitutive Equation for Concentrated Suspensions that Accounts for Shear-Induced Particle Migration," *Phys. Fluid.*, A 4, 30 .
16. Reinecke, N., et al. (1998). "Tomographic Imaging of the Phase Distribution in Two-Phase Slug Flow," *Int. J. Multiphase Flow*, 24, 617.
17. Vauhkonen, M. (1997). Electric Impedance Tomography and Prior Information, Ph.D. Thesis, Kupio University, Finland.
18. Vauhkonen, M., et al. (1998). "Tikhonov Regularization and Prior Information in Electrical Impedance Tomography," *IEEE Trans. Med. Imaging*, 17, 285.
19. Webster, J.G. (1990) "Electrical Impedance Tomography," Adams Hilger, Bristol.
20. Woo, E.J. (1990). "Finite Element Method and Reconstruction Algorithms in Electric Impedance Tomography," Ph.D. Thesis, University of Wisconsin-Madison
21. Chun, W, et. al. (2001). "Image Capturing of Dispersed Phases in DCHXs by Elerctric Tomography," Journal of the Korean Solar Energy Society, 21(2), 69.